Accepted Manuscript

The effect of silicon and ferrocene on the char formation of modified novolac resin with high char yield

Jin Yun, Lixin Chen, Xiaofei Zhang, Hui Zhao, Ziyou Wen, Chi Zhang

PII: S0141-3910(17)30071-X

DOI: 10.1016/j.polymdegradstab.2017.03.018

Reference: PDST 8192

To appear in: *Polymer Degradation and Stability*

Received Date: 24 December 2016

Revised Date: 23 March 2017

Accepted Date: 23 March 2017

Please cite this article as: Yun J, Chen L, Zhang X, Zhao H, Wen Z, Zhang C, The effect of silicon and ferrocene on the char formation of modified novolac resin with high char yield, *Polymer Degradation and Stability* (2017), doi: 10.1016/j.polymdegradstab.2017.03.018.

The effect of silicon and ferrocene on the char formation of modified novolac resin with high char yield

Jin Yun[1], Lixin Chen[1]*, Xiaofei Zhang[1], Hui Zhao[1], Ziyou Wen[1], Chi Zhang[1]

[1]Department of Applied Chemistry, School of Natural and Applied Sciences, Northwestern Polytechnical University, Xi'an 710072, PR China

*Correspondence: E-mail: lixin@nwpu.edu.cn

Abstract: Novolac resin (NR) modified with 1, 1'-bis(dimethylsilyl) ferrocene (FeNR) was synthesized. The thermal properties and structural evolution of cured FeNR were studied to analyze the reason for high char yield of cured FeNR. Thermal stability of cured FeNR has been improved, and the char yield of cured FeNR at 800^{o}C can be increased by 8.82% in comparison to that of cured NR. The results show that silicon atom and ferrocene contribute to the high char yield of cured FeNR. On one hand, the Si-O structure can be kept in the system during the whole pyrolysis process, which could help to reduce the weight loss. On the other hand, introducing ferrocene into novolac resin promotes the graphitization degree and graphite crystallites of pyrolyzed resins. Moreover, the pyrolyzed products possess different magnetic properties owing to the formation of iron nanocrystal at 800^{o}C and Fe_5Si_3 nanocrystal at 1200^{o}C.

Key words: novolac resin; 1, 1'-bis (dimethylsilyl) ferrocene; silicon; char yield; graphitization; magnetic material

1. Introduction

Phenolic resins (PF) are widely used in the aerospace industry, commodity and construction due to its low cost, superior flame resistance, ablative properties and high resistance against various solvents, acids and water and so on [1, 2]. Boron-containing compounds (BC_4 [3], boric acid [4]) are usually

introduced into PF to improve their thermal properties. Boric acid is widely used in phenolic resins modification according to the reaction of methyol group or phenolic hydroxyl group with boric acid. Based on the study of our previous work and other researches [5, 6], the formation of B_2O_3 helps to increase the thermal stabilities and char yield of modified resins. Moreover, introducing B into the system will improve the graphitization of the materials and is beneficial to the formation of an ordered structure during the pyrolysis process [6-9]. In spite of the observed thermal stability reinforcing effect, only partial hydroxyl of boron compounds can react with methylol and/or phenolic, and phenylborates are sensitive to the moisture [10].

Besides boron compounds, silicon-containing chemical additives have also been introduced into PF to enhance their thermal properties. Chiang and co-workers synthesized novolac/SiO_2 nanocomposites by sol-gel method, and both thermal and mechanical properties were improved [11]. In recent report, Li et al. also used the same method to synthesize silicone modified novolac resin. The result revealed that modified resin possessed better thermal stability and anti-oxidation properties [12]. This good thermal stability is considered to result from high bonding energy of Si-O structure in polymers [13].

Because graphitization structure can contribute to the good thermal properties [14, 15], catalysts such as Fe, Ni, Ti and Zr [16-23], as well as refractory-metal carbides TiC (titanium carbide), ZrC (zirconium carbide), VC (vanadium carbide), and WC (tungsten carbide) have been used for the graphitization of amorphous carbons at lower temperature [24-26]. But a heterogeneous morphology with metal-based particle grains is usually observed because of insolubility of the inorganic powder.

Ferrocene used as a kind of common organometallic compound has potentials to form iron nanocrystal during pyrolysis [27]. Here in this report, 1, 1’-bis (dimethylsilyl) ferrocene was chosen to

modify novolac resin because of its good solubility in resin and containing reactive Si-H groups. Novolac resin with different contents of 1, 1'-bis (dimethylsilyl) ferrocene was synthesized and their thermal property was studied. Then the chemical states of silicon and ferrocene during pyrolysis process were analyzed to discuss effects of silicon and ferrocene on the char formation of cured FeNR.

2. Experimental Section

2.1 Materials

Phenol, formaldehyde (37 wt %), organic acid of bivalent metal salt catalyst (Catalyst), hexamethylenetetramine (HMTA) were purchased from Tianjin Chemical Reagent Co., China. The 1, 1′-bis(dimethylsilyl) ferrocene was synthesized from ferrocene and chlorodimethylsilane as described previously [28]. All materials were of analytical grade and used as received without further purification.

2.2 Synthesis of FeNR

40.00g phenol, 24.15g formaldehyde and 0.80g Catalyst were added into 250 mL three-necked flask equipped with a stirrer, a reflux condenser, a thermometer. The system was stirred at 100^{o}C for 5h and 120^{o}Cfor 2h. After extraction of water, 1, 1'-bis (dimethylsilyl) ferrocene was added into the system and reacted for 5h at 90^{o}C and 4h at 102^{o}C. Finally, subjecting the system to a vacuum at 120°C for 40 to 50 minutes. FeNR with 5, 7.5, 10, 12.5 wt % of 1, 1'-bis (dimethylsilyl) ferrocene (based on the weight of neat novolac resin) were named after FeNR-5, FeNR-7.5, FeNR-10, FeNR-12.5, respectively.

2.3 Synthesis of NR

Adding the same dosage of phenol, formaldehyde and Catalyst into 250 mL three-necked flask, the system reacted at 100^{o}C for 8h and at 120^{o}C for 2h. Then exposure the system to a vacuum at 120°C for 50 minutes.

2.4 Preparation of the cured FeNR

Blend sample was prepared by mixing FeNR with 12% HMTA in ethanol under magnetic stirring at 50^{o}C for 2h until a homogenous solution was obtained. Then the solvent was evaporated at 60 °C under vacuum. The concentrated sample was cured in a vacuum oven at 115^{o}C for 2h, 125^{o}C for 2h and 180^{o}C for 3h.

2.5 Preparation of carbonized samples

The cured resins were placed in graphite crucible and were heated in tube furnace from 50^{o}C to the targeted temperatures (400^{o}C, 600^{o}C, 800^{o}C, 1000^{o}C, 1200^{o}C) for 2h in Ar with a heating rate of 10 ^{o}C/min.

2.6 Characterization

The structures of resins were analyzed by using FT-IR spectrometer (Bruker, Germany) with KBr pellets. ^{1}H NMR and ^{13}C NMR spectra of modified resin were recorded on a Bruker (Bruker Avence, Germany) 400MHz spectrometer. The deuterated dimethylsulfoxide-d_6 was used as a solvent. ^{29}Si NMR spectra were token in acetone solvent through an Inova 400MHz (America) instrument. The X-ray photoelectron spectroscopic (XPS) measurements were performed using a K-Alpha spectrometer (Thermo Fisher Scientific, Waltham, USA). The spectra were referenced to the C1s peak at 284.80 eV. A thermal gravimetric analyzer (TGA, STA 409T, Netzsch) was used to analyze the thermal properties of cured resins. The experiments were conducted under Ar atmosphere with a heating rate of 10^{o}C/min from 25^{o}C to 1200^{o}C. X-ray diffraction (XRD) patterns of pyrolyzed products of cured resins were obtained by using a Bruker D8 Advance (Bruker AXS, Germany, λ=0.154nm) in the 2θ range, 10–80°. XRD tests were used to illustrate the fine-phase structures and investigate the effects of modifier on the structural properties, as well as the graphite interlayer distance d_{002} [29]. Raman spectrometer (Renishaw 2000) associated with λ=514.5 nm was used to ascertain the I_D/I_G ratio (R) [30]. The magnetic properties of

samples were performed using a superconducting quantum interference device (SQUID, Lake Shore VSM 7307, America) at a temperature of 300 K.

3 Results and Discussion

3.1 Characterization of FeNR

The structures of modified resin were confirmed via FT-IR, ^{13}C NMR and XPS. Fig. 1a shows that the absorption bands assigned to the stretching vibration of Si-O-C group appears at 1008 cm^{-1}. This band was not observed in the NR FT-IR spectrum. The peak at 794 cm^{-1} corresponds to the stretching vibration of Si-C [31]. Peaks at 749 cm^{-1} and 818 cm^{-1} are attributed to the C-H out-of-plane bending vibration of ortho substituted and para substituted, respectively [32]. Peak at 1453 cm^{-1} is attributed to the vibration of C-H in methylene bridge [33]. Peaks around 1497 cm^{-1} and 1591 cm^{-1} corresponded to C=C aromatic ring vibration [34]. Fig. 1b presents ^{13}C NMR spectra of the modified resin, in which signals at -1.18 ~ -1.03 ppm for methyl of Si-CH_3 [35], 69.71 ppm for quaternary carbon of C_5H_4 section, 70.89 ppm and 71.17 ppm for the tertiary carbon of C_5H_4 section [28], 67.53~68.16 ppm for methylene of Si-O-CH_2 [36], 29.06 ppm~29.67 ppm for the ortho-ortho methylene bridge, 34.19~34.56 ppm for the ortho-para methylene bridge, 114.40 ppm~130.10 ppm for the CH=CH of the benzene rings and 152.01 ppm ~ 157.14 ppm for the quaternary carbon of benzene rings were collected [37]. In Fig. 1c-d, the existence of iron and silicon in the modified resin were further confirmed by the Fe2p and Si2p XPS spectra. They were acquired to analyze the chemical state of silicon and iron in the modified resin. The deconvolution of Si2p spectrum presents one peak centered at 102.35 eV which is associated with R_3Si-O-C bonding. 708.55eV is the Fe 2p3/2 peak and 720.70eV is the Fe 2p1/2 peak from ferrocene unit, which shows the existence of the ferrocene structure [38, 39].

Fig. 1 (a) FT-IR spectra for the FeNR with different modifier contents; (b) ^{13}C NMR spectrum of FeNR-12.5; (c) Si2p spectrum of FeNR-12.5 ; (d) Fe2p spectrum of FeNR-12.5.

The structures of cured modified resin and cured novolac resin are analyzed by FT-IR and XPS spectra. In Fig. 2a, peaks at about 1630 cm^{-1} and 1206 cm^{-1} are the deformation and stretching vibration of C-N, respectively [40, 41]. The stretching vibration of N-H in NC_2H is overlapped with that of O-H in phenol at about 3400 cm^{-1}. N atom exists in at least two different chemical environments which could be attributed to NC_3 and NC_2H. In Fig. 3b and Fig. 3f, peak at 401.00eV is assigned to NC_3. Peaks at 399.60 eV and 399.90 eV can be ascribed to NC_2H structure in cured NR and FeNR-7.5, respectively [33, 42-44]. 708.55 eV and 721.20 eV are assigned to Fe 2p3/2 peak and Fe 2p1/2 peak from ferrocene units, respectively. Peak at 102.31 eV represents Si-O-C structure in the cured modified resin. Si-Ox is the oxidation of modified resin surface [45, 46]. According to analyses above, the synthetic method and the structure of cured resin were shown in Fig. 4.

Fig. 2 (a) FT-IR spectra of NR; (b) FT-IR spectra of FeNR-7.5.

Fig. 3 (a) The XPS spectrum of cured NR; (b) N1s spectrum of cured NR; (c) The XPS spectrum of cured FeNR-7.5; (d) Si2p spectrum of cured FeNR-7.5; (e) Fe2p spectrum of cured FeNR-7.5; (f) N1s spectrum of cured FeNR-7.5.

Fig. 4 The synthetic method of FeNR and cured FeNR

3.2 Thermal properties of FeNR

The effect of 1, 1'-bis (dimethylsilyl) ferrocene on the thermal properties of modified resin was measured by TGA in Fig. 5a and the corresponding data were collected in Table 1. According to the data in Table 1, the temperature at 5% weight loss ($T_{5\%}$), the temperature at maximum weight loss (T_{max}) and the char yield of modified resins at 800°C, 1000°C and 1200°C are all higher than that of cured NR. Char yields of cured FeNR-7.5 at 800°C (C_{800}=69.99%), 1000°C (C_{1000}=63.17%) and 1200°C (C_{1200}=56.34%) can be nearly increased by 8.8%, 14.1% and 20.0%, respectively, in comparison to that of cured NR. Previous studies have been shown that the bonding energy of Si-O (423kJ/mol) is higher than that of C-O (384kJ/mol) and C-C bonds [16], resulting in fracture of Si-O bond at higher temperature. Thus, less weight loss for cured FeNR can be partially attributed the formation of Si-O bond. As has been mentioned above, Fe can catalyze the graphitization of amorphous carbons at lower temperature and the graphitization structure can contribute to the good thermal properties. So enhanced char yield could also be ascribed to the formation of graphitization structure induced by iron nanopartilces from pyrolysis of ferrocene units. It is noticeable that when the contents of modifier increase to 10 % and 12.5%, the char yields were lower than that of cured FeNR-7.5. In order to explain the phenomena, ^{1}H NMR and ^{29}Si NMR measurements were used and the related structures were further analyzed. Methyl methacrylate (MMA) is used as a reference to calculate the content of methylol groups. In Fig. S1, results show that the concentration of methylol group in novolac resin intermediate is 1.05mmol/g. For novolac resin intermediate adding 7.5 % and 12.5 % of 1, 1'-bis (dimethylsilyl) ferrocene, their Si-H contents are 0.496mmol/g and 0.827mmol/g, respectively. After introducing modifier into the system, methylol groups not only react with Si-H groups, but also with methylol groups or the active site on the phenol groups. In Fig. 5b, peak at 9.00 ppm is ascribed to Si-O-Si structure and the peak at 11.65 ppm is Si-O-C structure [47]. According to the ^{29}Si NMR results, there is Si-O-Si structure in FeNR-12.5 besides Si-O-C structure. The Si-O-Si structure might be from oligomer which is produced by the reaction between partial modifiers and water in the system [48]. The reactions are shown below:

$$\equiv Si{-}H + H_2O \longrightarrow \equiv Si{-}OH + H_2$$

$$\equiv Si{-}OH + \equiv Si{-}OH \longrightarrow \equiv Si{-}O{-}Si\equiv + H_2O$$

Therefore, when the content of modifier exceeds 7.5%, some modifiers will take part in the formation of oligomer and consequently reduce the char yield.

Fig. 5 (a) TGA curves of cured FeNR from room temperature to 1200^{o}C with a heating rate of 10^{o}C/min under Ar atmosphere; (b) ^{29}Si NMR spectra of FeNR-7.5 and FeNR-12.5.

Table 1 TGA data of cured NR and cured FeNR

Table 2 Char yields of cured novolac resin modified with different additives at 800 ^{o}C

Table 2 shows the char yields of novolac resin modified with different additives according to references. Nanoclay and GO have been introduced successfully to modify novolac resin. Zhang's group synthesized phenolic resin/clay nanocomposites and the C_{800} of novolac resin with 4.2 wt % modifier increased by 5.0% [49]. Zhao et al. synthesized RGO-PF composites and the C_{800} of modified novolac resin increased by 8.0% with 1.0 wt % oxide graphene in comparison to that of neat novolac resin [50]. In the case of boron-containing additives, phenylboronic acid was used to improve char yield of novolac resin in our previous work. The result showed that the C_{800} of resin with 38.9 wt % modifier improved by 5.4% [5]. Silicon-containing novolac resin was prepared by Li's group using KH560, DMDMS and PTMS as modifiers. They reported that when the weight ratio between m-NR and SI is 65:35, C_{800} of modified resin can increase to 71.0% and the C_{800} of neat novolac is 60.0% [51]. They also only used methyltrimethoxysilane to modify novolac resin and C_{800} increased by 5.0% after adding 131.7wt % modifier [12]. In a similar work, boric acid using as curing agent was introduced into silicon-containing resin. The results showed that C_{800} of modified resin improved by 5.5% [52]. Though the char yields have been improved significantly, the contents of modifiers are high. In the current study, we showed that after adding 7.5% of modifier, the char yield at 800^{o}C improved by 8.8% and the pyrolysis products possessed

magnetic properties which might have other potential applications.

3.3 The effects of Si and ferrocene on the char formation

3.3.1 Analysis of XPS

In order to confirm the presence of silicon in the cured resin and to estimate the chemical state during the pyrolysis process, XPS measurements were made as shown in Fig. 6. The products of cured FeNR-7.5 pyrolyzed at 400^{o}C, 600^{o}C, 800^{o}C, 1000^{o}C and 1200^{o}C are named as FeNR-400, FeNR-600, FeNR-800, FeNR-1000 and FeNR-1200, respectively. The products of cured NR pyrolyzed at 400^{o}C, 600^{o}C, 800^{o}C, 1000^{o}C and 1200^{o}C are named as NR-400, NR-600, NR-800, NR-1000 and NR-1200, respectively.

Fig. 6 The XPS analyses of cured NR and cured FeNR-7.5 pyrolyzed at 800^{o}C, 1000^{o}C and 1200^{o}C under Ar atmosphere: (a) XPS spectra of cured NR and cured FeNR-7.5 (red line: the XPS spectra of cured NR; black line: the XPS spectra of cured FeNR-7.5)； (b) Si 2p spectra of cured FeNR-7.5.

Fig. 6 is the XPS spectra of cured NR and FeNR pyrolyzed at 800^{o}C, 1000^{o}C and 1200^{o}C to confirm the existence of elements and to estimate chemical states of silicon at different heating temperatures. As shown in Fig. 6a, XPS analyses show there are carbon and oxygen in pyrolyzed products of cured NR. Si exists in the cured FeNR during the pyrolysis process, besides carbon and oxygen elements. There is no evidence showing the existence of ferrocene or iron compounds owing to the low content of modifier. In Fig. 6b, peaks at 102.28 ~ 102.70 eV are assigned to Si-O-C structure which can be seen at 800^{o}C, 1000^{o}C and 1200^{o}C. Peaks at 103.65 eV, 103.70 eV and 103.80 eV are the Si-O_x which can be attributed to the oxidation of modified resin surface before measurement or the

oxygen from the argon atmosphere [53-55].

3.3.2 Analysis of XRD

The powder XRD patterns of samples prepared by pyrolysis of cured FeNR and cured NR at 400^{o}C, 600^{o}C, 800^{o}C, 1000^{o}C and 1200^{o}C in Fig. 7 are shown to illustrate the fine-phase structures and to investigate the effects of modifier on the structural properties during the pyrolysis process. With the temperature rising, the orderliness of the carbonized product structures in cured resins increased, especially for that of cured FeNR. The crystallinity of cured FeNR was dramatically improved.

In Fig. 7, when the treating temperature is 400^{o}C and 600^{o}C, there is a broad peak at around 18°, which is ascribed to the adjacent chains of linear polymer [6]. When the treating temperature increases from 800^{o}C to 1200^{o}C, diffraction peaks of (002) and (100) for pyrolyzed products of cured FeNR-7.5 in Fig. 7b are more obvious than that of pyrolyzed products of cured NR in Fig. 7a. The site and width of (002) peaks are associated with the variation in the interlayer spacing [56, 57]. The crystallite parameters of pyrolyzed products are listed in Table 3. As can be seen, for pyrolyzed products of cured FeNR-7.5, the (002) peak of the graphite is observed at 25.88°, 25.91° and 25.88° when pyrolysis temperature is from 800^{o}C to 1200^{o}C, respectively. The d_{002}-spacings of sample FeNR-800, FeNR-1000 and FeNR-1200 can be decreased to 0.344nm. For cured NR, the lowest d_{002} spacing of pyrolyzed product is 0.3759. Thus, the results indicate that introducing ferrocene can accelerate graphitization of the materials.

In Fig. 7 b, for sample FeNR-800, the diffraction peaks at 43.71° is indexed to the Fe (111) (ICSD, PDF23-0298). The peak at 44.69° is Fe (110) (ICSD, PDF87-0721). These two kind of fine-phase structures also exist in sample FeNR-1000. Besides, the phase SiC (111) (ICSD, PDF74-2307) also exists in sample FeNR-1000. For FeNR-1200 sample, diffraction peaks at 40.83°, 45.21° and 46.94°

are corresponding to the Fe_5Si_3 (210), (211) and (300) (ICSD,PDF65-3593), respectively. According to analyses above, silicon in the system was partially transformed into SiC nanocrystal in pyrolysis process at 1000^{o}C. However, SiC is totally unstable in the presence of iron, because it will react with iron to form Fe_5Si_3 nanocrystal and free carbon [58]. So when pyrolysis temperature was higher than 1000^{o}C, the SiC together with iron nanocrystal were converted to Fe_5Si_3. During the pyrolysis process, ferrocene unit can be transformed into iron at 800^{o}C. When treating temperature is at 1200^{o}C, Fe_5Si_3 is formed through the reaction of iron and SiC nanocrystals.

Fig. 7 The XRD spectra of cured NR and cured FeNR-7.5 pyrolyzed at different temperatures: (a) NR; (b) FeNR-7.5.

Table 3 XRD and Raman Spectra results of cured NR and FeNR-7.5 treated at different temperatures

3.3.3 Analysis of Raman Spectra

Fig. 8 represents the Raman spectra of cure NR and cured FeNR-7.5 pyrolyzed at different temperatures. As can be seen, all the samples display two distinguishable peaks in the range of 1000−2000 cm^{-1}, one peak centered at about 1350 cm^{-1} (D band), and the other one at about 1590 cm^{-1} (G band). The Gaussian-Lorentzian curve fitting of Raman bands has been used to calculate the R value [59, 60]. R (I_D/I_G) which have shown in Table 3 is the intensity ratio of the D band to that of the G band, and it is used to determine the degree of crystallinity of carbon materials. With the increase of treating temperatures, the R values of all samples decrease, especially for pyrolyzed products of cured FeNR-7.5. The R values of pyrolyzed FeNR-7.5 decline from 1.650 to 1.339, and the R values of pyrolyzed NR decrease from 2.262 at 800^{o}C to 1.846 at 1200^{o}C. Thus, introducing ferrocene helps to

promote the transition of free carbon from disordered to ordered states in pyrolysis process.

Fig. 8 Raman spectra of (a) cured NR; (b) cured FeNR-7.5 pyrolyzed at 600 ^{o}C, 800^{o}C, 1000^{o}C and 1200^{o}C.

Through the above analyses, it is found that using 1, 1'-bis (dimethylsilyl) ferrocene to modify novolac resin could obviously improve the char yields. The increased char yields of modified novolac resin can be attributed to two factors, first, the high binding energy of Si-O in modified novolac resin imparts it with good heat resistance, which help to reduce the weight loss; second, previous studies have been reported that iron nanoparticle formed from ferrocene structure can be used as nucleators to induce the formation of organized structures during the pyrolysis process [61, 62]. As has been shown in XRD and Raman spectra, incorporation of ferrocene in resin can induce the formation of graphite structure at lower pyrolysis temperature. This more order structure has good thermal resistance which could help to reduce the weight loss at high pyrolysis temperature.

3.3.4 Analysis of Magnetic Property

After treating cured FeNR-7.5 at different pyrolysis temperatures, sample FeNR-800, FeNR-1000 and FeNR-1200 have response to an external magnetic field. The magnetic property of pyrolyzed cured resin was studied on a superconducting quantum interference device (SQUID) magnetometer at a temperature of 300 K. Fig. 9 shows the magnetization curves for the sample FeNR-800, FeNR-1000 and FeNR-1200. The saturation magnetization (*Ms*) value of sample FeNR-800 is 1.90 emu/g and the inset of Fig. 9 shows the coercivity (H_C) value and the remanence (*Mr*) value are 537.00 Oe and 0.82 emu/g, respectively. The *Ms* value, *Mr* value and H_C value for sample FeNR-1000 are 1.16emu/g, 0.38 emu/g and 450.56 Oe. The reason for a decrease of *Ms* is the partial consumption of iron nanocrystal

and the formation of Fe_5Si_3. For sample FeNR-1200, *Ms* value, *Mr* value and H_C value are 1.35 emu/g, 0.17 emu/g and 47.21 Oe. For all samples, *Mr* and H_C values of FeNR-1200 are lower than that of sample FeNR-800 and FeNR-1000.

Fig. 9 Magnetic hysteresis loops of sample FeNR-800, FeNR-1000, and FeNR-1200 at 300 K (inset: enlarged portion of the plots at low H)

4. Conclusion

The FeNR was synthesized by one-pot method using 1, 1'-bis (dimethylsilyl) ferrocene as a modifier. The char yields of cured FeNR at 800^{o}C,1000^{o}C and 1200^{o}C are all higher than that of cured NR. When the content of modifier is 7.5%, C_{800} can be increased by 8.82% compared with that of cured NR. Not only has the silicon atom contributed to the higher char yield, but also the catalysis of ferrocene. By introducing ferrocene, the d_{002}-spacing of FeNR-800 is 0.3440nm which is lower than that of NR-1200 (0.3801nm). R values of cured FeNR-7.5 at different pyrolysis temperatures decrease from 1.650 to 1.339. For the pyrolyzed products of cured NR, the R values reduce from 2.262 to 1.846. Iron, SiC, Fe_5Si_3 nanocrystals and graphite structure can be found when the pyrolysis temperature is from 800^{o}C to 1200^{o}C. Moreover, magnetic materials which have been formed during pyrolysis process could have the potential for practical applications in electromagnetic system, information storage and magnetic refrigeration.

Acknowledgements

This research did not receive any specific grant from funding agencies in the public, commercial, or not-for-profit sectors.

Reference

[1] Y. Fang, H. Zhang, X. Li, H. Ma, X. Li, Z. Yu, In situ chemical reduction and functionalization of graphene oxide for electrically conductive phenol formaldehyde composites, Carbon 68 (2014) 653-661.

[2] C. P. Reghunadhan Nair, Advances in addition-cure phenolic resins, Prog. Polym. Sci. 29 (2004) 401–498.

[3] J. Wang, J. Nan, H. Jiang, Micro-structural evolution of phenol-formaldehyde resin modified by boron-carbide at elevated temperatures, Mater. Chem. Phys. 120 (2010) 187-192.

[4] D. Wang, G. Chang, Y. Chen, Preparation and thermal stability of boron-containing phenolic resin/ clay nanocomposites, Polym. Degrad. Stabil. 93 (2008) 125-133.

[5] J. Yun, L. Chen, X. Zhang, J. Feng, L. Liu, The effect of introducing B and N on pyrolysis process of high ortho novolac resin, Polymers 8 (2016) 1-17.

[6] S. Wang, Y. Wang, B. Cheng. Y. Zhong, X. Jing, The thermal stability and pyrolysis mechanism of boron-containing phenolic resins: The effect of phenyl borates on the char formation, Appl. Surf. Sci. 331 (2015) 519-529.

[7] Y. Liu, X. Jing, Pyrolysis and structure of hyperbranched polyborate modified resins, Carbon 45 (2007) 1965-1971.

[8] S. Wang, X. Jing, Y. Wang, J. Si, High char yield of aryl boron-containing phenolic resins: The effect of phenylboronic acid on the thermal stability and carbonization of phenolic resins, Polym. Degrad. Stabil. 99 (2014) 1-11.

[9] H. Wang, Q. Gao, J. Yang, Z. Liu, Y. Zhao, J. Li, Z. Feng, L. Liu, Microstructural evolution and oxidation resistance of polyacrylonitrile-based carbon fibers doped with boron by the decomposition of

BC_4, Carbon 56 (2013) 296-308.

[10] M. Abdalla, A. Ludwick, T. Mitchell, Boron-modified phenolic resins for high performance applications, Polymer 44 (2003) 7353-7359.

[11] C. Chiang, C. M. Ma, D. Wu, H. Kuan, Preparation, characterization, and properties of novolac-type phenolic/SiO_2 hybrid organic-inorganic nanocomposite materials by sol-gel method, J. Polym. Sci. Pol. Chem. 41 (2003) 905 – 913.

[12] S. Li, Y. Han, F. Chen, Z. Luo, H. Li, T. Zhao, The effect of structure on thermal stability and anti-oxidation mechanism of silicone modified phenolic resin, Polym. Degrad. Stabil. 124 (2016) 68-76.

[13] J. E. Mark, Some interesting things about polysiloxanes, Accounts Chem. Res. 37 (2004) 946-953.

[14] H. Cheng, H. Xue, G. Zhao, C. Hong, X. Zhang, Preparation, characterization and properties of graphene-based composite arogels via in situ polymerization and three-dimensional self-assembly from graphene oxide solution, RSC Adv. 6 (2016) 78538-78547.

[15] J. Si, J. Li, S. Wang, Y. Li, X. Jing, Enhanced thermal resistance of phenolic resin composites at low loading of graphene oxide, Compos. Part A: Appl. S. 54 (2013) 166-172.

[16] D. G. Hall, Boronic acid: preparation and applications in organic synthesis, medicine and materials. New York: Wiley, 2012.

[17] S. Xu, F. Zhang, Q. Kang, S. Liu, Q. Cai, The effect of magnetic field on the catalytic graphitization of phenolic resin in the presence of Fe–Ni, Carbon 47 (2009) 3233-3237.

[18] H. Marsh, A. Warburton, Catalytic graphitization of carbon using titanium and zirconium, Carbon 14 (1976) 47–52.

[19] A. Oya, S. Otani, Catalytic graphitization of carbons by various metals, Carbon 17 (1979)

131–137.

[20] S. Park, S. Jo, D. Kim, W. Lee, B. Kim, Effects of iron catalyst on the formation of crystalline domain during carbonization of electrospun acrylic nanofiber, Synth. Met. 150 (2005) 265–270.

[21] W. Weisweiler, N. Subramanian, B. Terwiesch, Catalytic influence of metal melts on the graphitization of monolithic glasslike carbon, Carbon 9 (1971) 755–761.

[22] S. Tzeng, Catalytic graphitization of electroless Ni–P coated PAN-based carbon fibers, Carbon 44 (2006) 1986–1993.

[23] A. Mochizukai, An electron microscopic study on the turbostratic carbon formed in phenolic resin carbon by catalytic action of finely dispersed nickel, Carbon 17 (1979) 71–76.

[24] X. Hu, G. Cheng, B. Zhao, H. Wang, K. Hu, Catalytic effect of dopants on microstructure and performance of MCMB derived carbon laminations, Carbon 42 (2004) 381–386.

[25] C. Garcia-Rosales, N. Ordas, E. Oyarzabal, J. Echeberria, M. Balden, S. Lindig, Improvement of the thermo-mechanical properties of fine grain graphite by doping with different carbides, J. Nucl. Mater. 307 (2002) 1282–1288.

[26] H. Qiu, Y. Song, L. Liu, G. Zhai, J. Shi, Thermal conductivity and microstructure of Ti-doped graphite, Carbon 42 (2003) 973–978.

[27] C. H. W. Kelly, M. Lein, Choosing the right precursor for thermal decomposition solution-phase synthesis of iron nanoparticles: tunable dissociation energies of ferrocene derivatives, Phys. Chem. Chem. Phys. 18 (2016) 32448-32457.

[28] J. Kong, T. Schmalz, G. Motz, A. Müller, Novel hyperbranched ferrocene-containing poly(boro)carbosilanes synthesized via a convenient "A_2B_3" approach, Macromolecules 14 (2011) 1280-1291.

[29] M. Endo, C. Kim, T. Karaki, T. Tamaki, Y. Nishimura, M. J. Matthews, S. D. M. Brown, M. S. Dresselhaus, Structural analysis of the B-doped mesophase pitch-based graphite fibers by Raman spectroscopy, Phys. Rev. B. 58 (1998) 8991-8996.

[30] F. Tuinstra, J. K. Koening, Ranman spectrum of graphite, J. Chem. Phys. 53 (1970) 1126-1130.

[31] X. Pu, H. Zhang, X. Li, C. Gui, Z. Yu, Thermally conductive and electrically insulating epoxy nanocomposites with silica-coated graphene, RSC Adv. 4 (2014) 15297-15303.

[32] I. Poljanšek, M. Krajnc, Characterization of phenol-formaldehyde prepolymer resins by in line FT-IR spectroscopy, Acta. Chim. Slov. 52 (2005) 238-244.

[33] M. Strečková, Ľ. Medvecký, J. Füzer, P. Kollár, R. Bureš, M. Fáberová, Design of novel soft magnetic composites based on Fe/resin modified with silica, Mater. Lett. 101 (2013) 37-40.

[34] Y. Cheng, J. Yang, Y. Jin, D. Deng, F. Xiao, Synthesis and properties of highly cross-linked thermosetting resins of benzocyclobutene-functionalized benzoxazine, Macromolecules 45 (2012) 4085–4091.

[35] J. Miravet, J. Fréchet, New hyperbranched poly(siloxysilanes) variation of the branching pattern and end-functionalization, Macromolecules 31 (1998) 3461–3468.

[36] S. Niu, H. Yan, Novel sillicone-based polymer cotaining active methylene designed for the removal of indoor formaldehyde, J. Hazard. Mater. 287 (2015) 259–267.

[37] M. Nomoto, Y. Fujikawa, T.Komoto, T. Yamanobe, Structure and curing mechanism of high ortho novolac resin as studied by NMR, J. Mol. Struct. 976 (2010) 419–426.

[38] C. Woodbridge, D. L. Pugmire, R. Johnson, N. Boag, M. Langell, Hreels and XPS studies of ferrocene on Ag(100), J. Phys. Chem. B . 104 (2000) 3085-3093.

[39] A. Fischer, M. Wrighton, M. Umana, R. Murray, An X-ray photoelectron spectroscopic study of

multilayers of an electroactive ferrocene derivative attached to platinum and gold electrodes, J. Am. Chem. Soc. 101 (1979) 3442–3446.

[40] Y. Wang, S. Wang, C. Bian, Effects of chemical structure and cross-link density on the heat resistance of phenolic rensin, Polym. Degrad. Stabil. 111 (2015) 239-246.

[41] D. Wang, B. Li, Y. Zhang, Z. Lu, Triazine-containing benzoxazine and its high-performance polymer, J. Appl. Polym. Sci. 127 (2013) 516-522.

[42] B. Wang, Y. Huang, L. Liu, Effect of solvents on adsorption of phenolic resin onto γ-aminopropyl-triethoxysilane treated silica fiber during resin transfer molding, J. Mater. Sci. 41 (2006) 1243-1246.

[43] T. Iwazaki, R. Obinata, W. Sugimoto, High oxygen-reduction activity of silk-derived activated carbon, Electrochem. Commun. 11 (2009) 376-378.

[44] B. Ashourirad, A. Sekizkardes, S. Altarawneh, H. El-Kaderi, Exceptional gas adsorption properties by nitrogen-doped porous carbons derived from benzimidazole-linked polymers, Chem. Mater. 27 (2015) 1349–1358.

[45] H. Yan, S. Li, Y. Jia, X. Ma, Hyperbranched polysiloxane grafted graphene for improved tribological performance of bismaleimide composites, RSC Adv. 5 (2015) 12578-12582.

[46] J. Kong, M. Kong, X. Zhang, L. Chen, L. An, Magnetoceramics from the bulk pyrolysis of polysilazane cross-linked by polyferrocenylcarbosilanes with hyperbranched topology, ACS Appl. Mater. Interfaces 5 (2013) 10367–10375.

[47] S. O'Brien, J. M. Keates, S. Barlow, M. J. Drewitt, B. R. Payne, D. O'Hare, Synthesis and characterization of ferrocenyl-modified mesoporous silicates. Chem. Mater. 10 (1998) 4088–4099.

[48] M. Schiavon, N. Armelin, I. Yoshida, Novel poly(borosiloxane) precursors to amorphous SiBCO

ceramic, Mater. Chem. Phys. 112 (2008) 1047–1054.

[49] Z. Zhao, G. Ye, H. Toghiani, C. U. Pittman Jr., Morphology and thermal stability of novolac phenolic resin/clay nanocomposites prepared via solution high-shear mixing, Macromol. Mater. Eng. 295 (2010) 923-933.

[50] X. Zhao, Y. Li, J. Wang, Z. Ouyang, J. Li, G. Wei, Z. Su, Interactive oxidation-reduction reaction for the in situ synthesis of graphene-phenol formaldehyde composites with enhanced properties, ACS Appl. Mater. Interfaces 6 (2014) 4254-4263.

[51] S. Li, F. Chen, Y. Han, H. Zhou, H. Li, T. Zhao, Enhanced compatibility and morphology evolution of the hybrids involving phenolic resin and silicone intermediate, Mater. Chem. Phys. 165 (2015) 25-33.

[52] S. Li, F. Chen, B. Zhang, Z. Luo, H. Li, T. Zhao, Structure and improved thermal stability of phenolic resin containing silicon and boron elements, Polym. Degrad. Stabil. 133 (2016) 321-329.

[53] X. Zhang, L. Chen, L. Meng, F. Chen, J. Kong, Nickel silicide nanocrystal-containing magnetoceramics from the bulk pyrolysis of polysilazane and nickelocene, Ceram. Int. 40 (2014) 6937-6947.

[54] R. Williams, G. Kelsall, An investigation of the surface properties of atomized Fe_xSi powders, J. Colloid Interf. Sci. 32 (1989) 210-219.

[55] S. Saha, R. Howell, M. Hatalis, Silicidation reactions with Co-Ni bilayers for low thermal budget microelectronic applications, Thin Solid Films 347 (1999) 278-283.

[56] I. Norio, R. Chong, F. Hiroyuki, Specification for a standard procedure of X-ray diffraction measurements on carbon materials, Carbon 42 (2004) 701-714.

[57] S. Lyu, J. Han, K. Shin, Synthesis of boron-doped double-walled carbon nanotubes by the

catalytic decomposition of tetrahydrofuran and triisopropyl borate, Carbon 49 (2011) 1532-1541.

[58] Y. Pan, J. Baptista, Chemical instability of silicon carbide in the presence of transition metals, J. Am. Ceram. Soc. 79 (1996) 2017-2026.

[59] J. Kong, M. Wang, J. Zou, L. An, Soluble and meltable hyperbanched polyborosilazanes toward high-tempertaure stable SiBCN ceramics, Appl. Mater. Interfaces 7 (2015) 6733–6744.

[60] A. Ferrari, J. Robertson, Interpretation of Raman spectra of disordered and amorphous carbon, Phys. Rev. B. 61 (2000) 14095-14107.

[61] M. G. Segatelli, E. Radovanovic, M. C. Gonçalves, I. V. P. Yoshida, Investigation of the morphological changes promoted by heating of Si-O-C ceramics derived from a phenyl-rich hybrid polymer. Effect of Ni in the polymeric precursor, J. Eur. Ceram. Soc. 29 (2009) 3279-3287.

[62] Y. Lu, Z. Zhu, Z. Liu, Carbon-encapsulated Fe nanoparticles from detonation-induced pyrolysis of ferrocene, 43 (2005) 369-374.

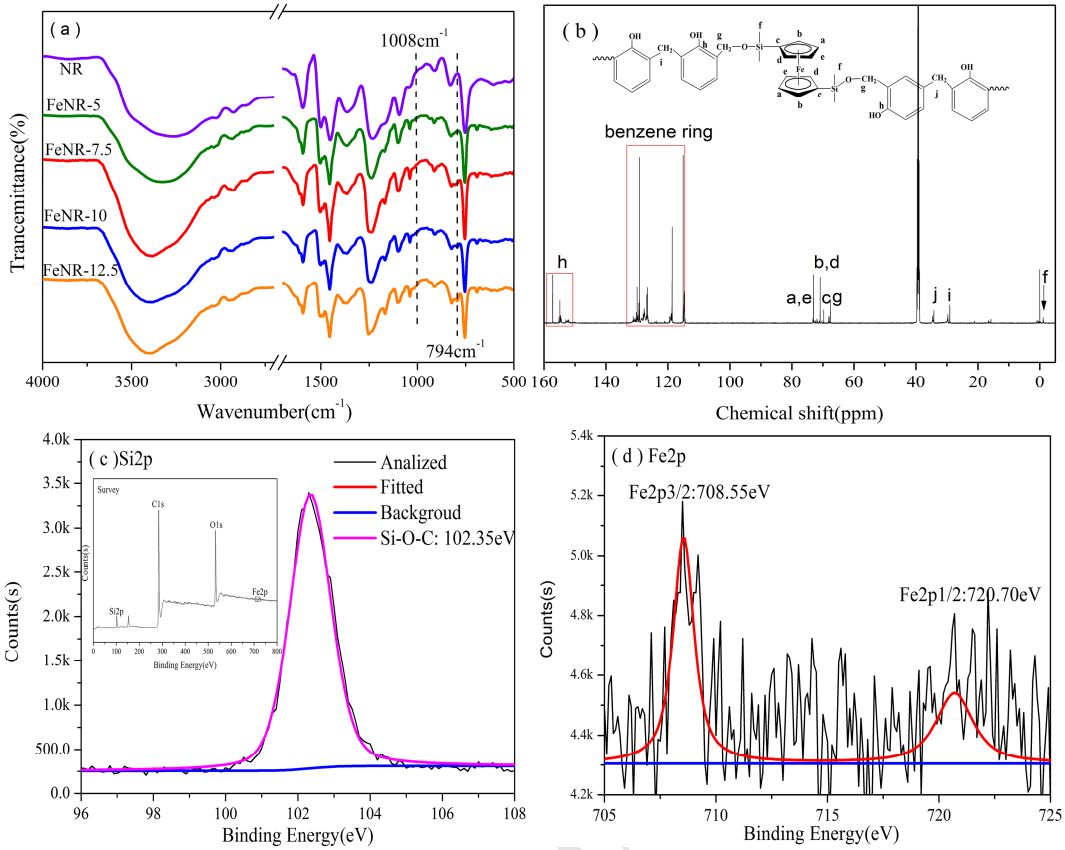

Fig. 1 (a) FT-IR spectra for the FeNR with different modifier contents; (b) ^{13}C NMR spectrum of FeNR-12.5; (c) Si2p spectrum of FeNR-12.5 ; (d) Fe2p spectrum of FeNR-12.5.

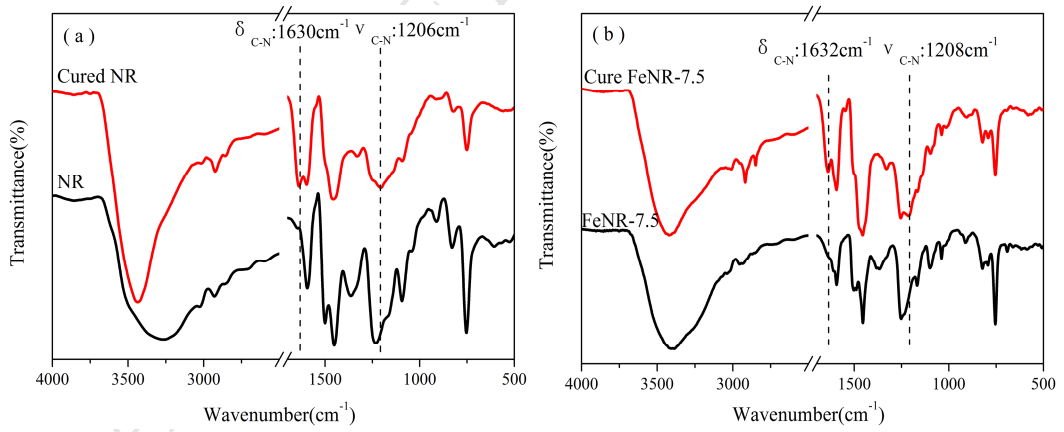

Fig. 2 (a) FT-IR spectrum of NR; (b) FT-IR spectrum of FeNR-7.5.

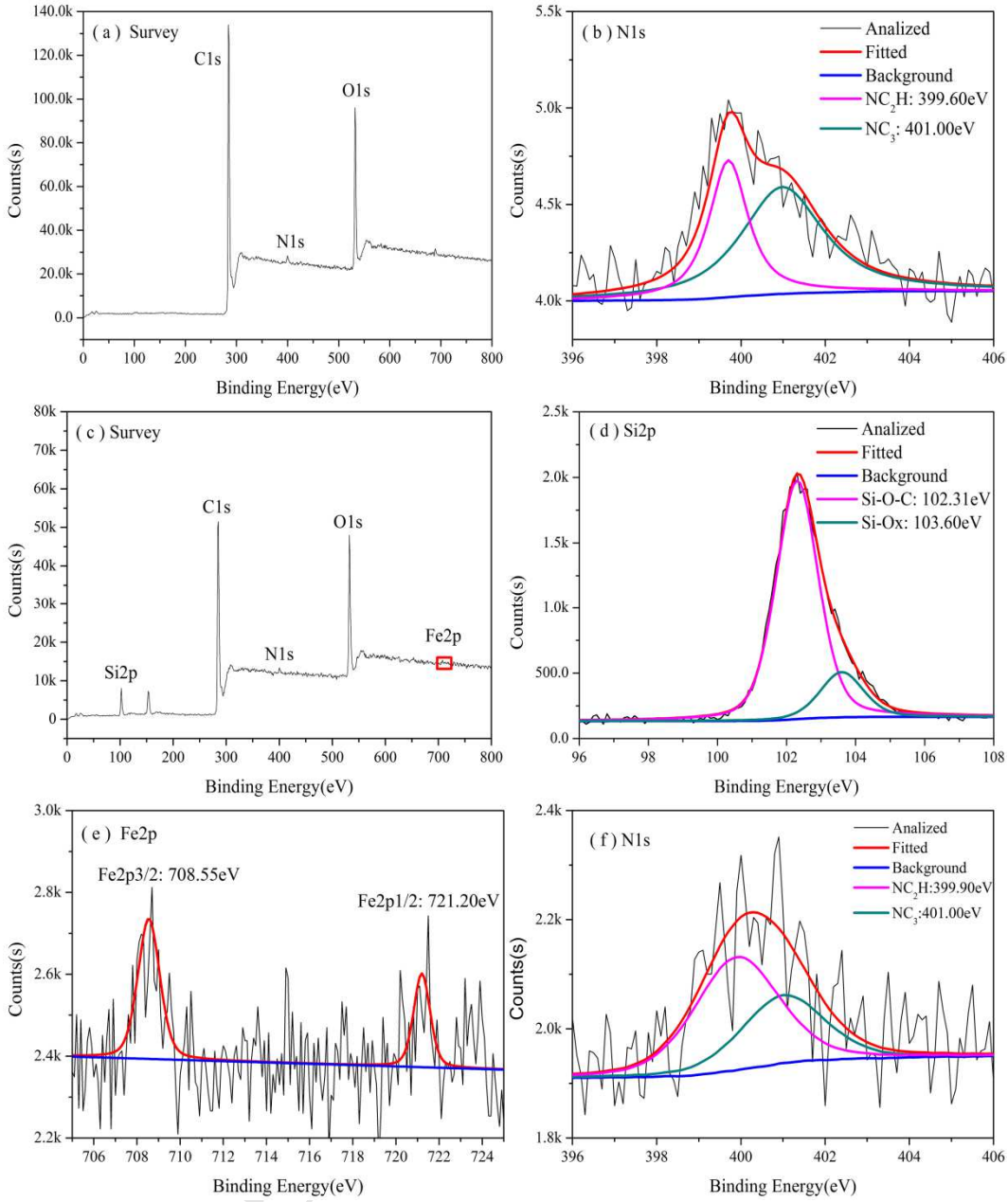

Fig. 3 (a) The XPS spectrum of cured NR; (b) N1s spectrum of cured NR; (c) The XPS spectrum of FeNR-7.5; (d) Si2p spectrum of cured FeNR-7.5; (e) Fe2p spectrum of cured FeNR-7.5; (f) N1s spectrum of cured FeNR-7.5.

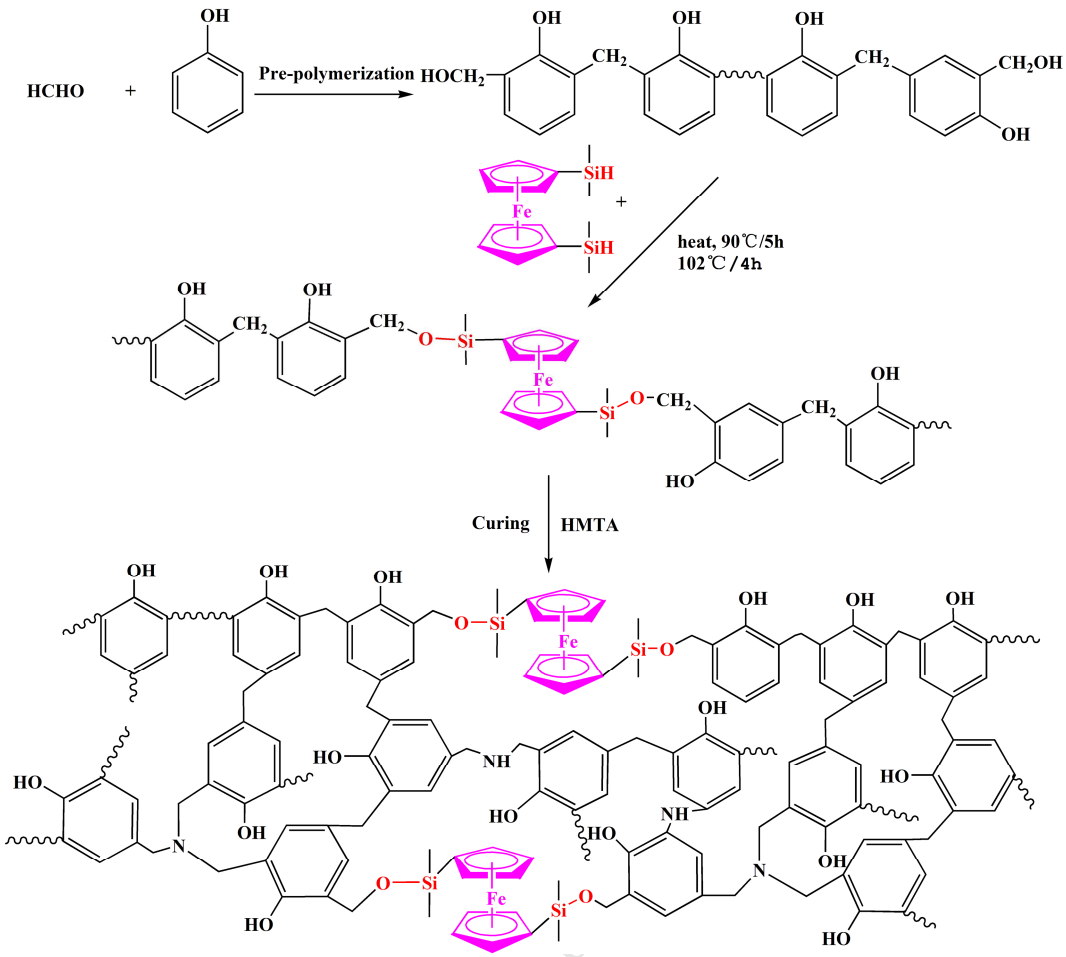

Fig. 4 The synthetic method of FeNR and cured FeNR

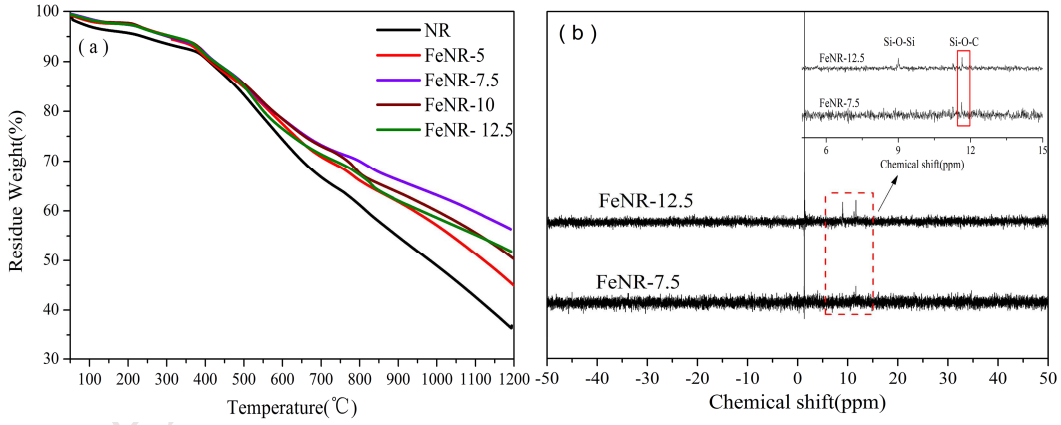

Fig. 5 (a) TGA curves of cured FeNR from room temperature to 1200°C with a heating rate of 10°C/min under Ar atmosphere; (b) ^{29}Si NMR spectra of FeNR-7.5 and FeNR-12.5.

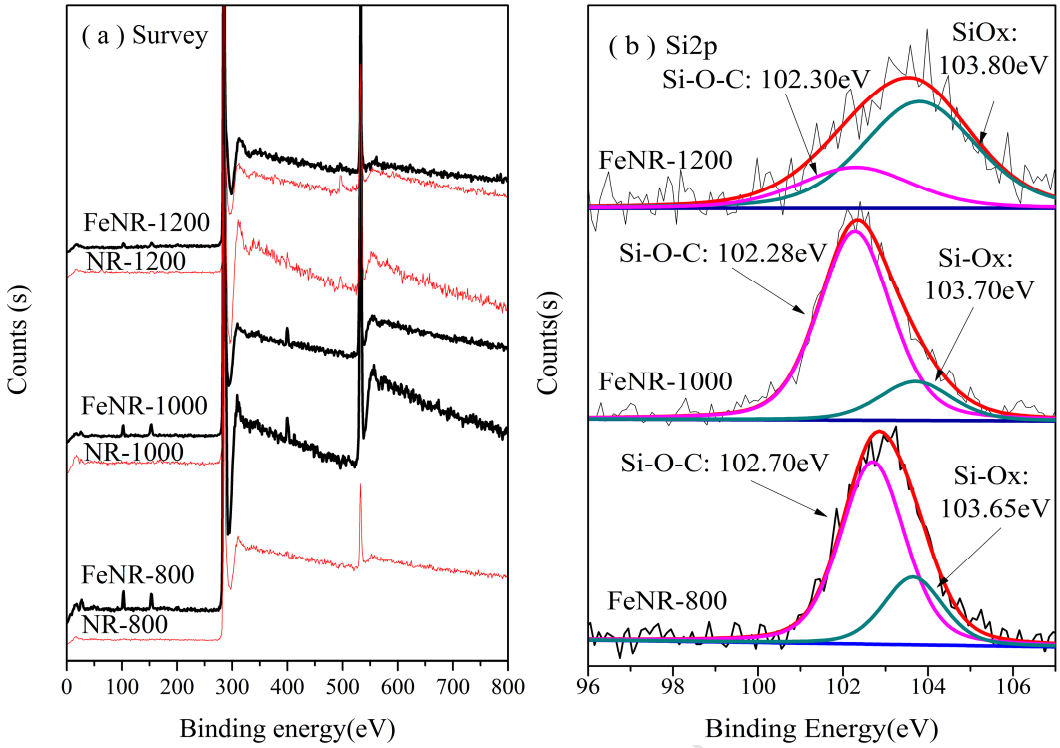

Fig. 6 The XPS analyses of cured NR and cured FeNR-7.5 pyrolyzed at 800°C, 1000°C and 1200°C under Ar atmosphere: (a) XPS spectra of cured NR and cured FeNR-7.5(red line: the XPS spectra of cured NR; black line: the XPS spectra of cured FeNR-7.5)； (b) Si 2p spectra of cured FeNR-7.5.

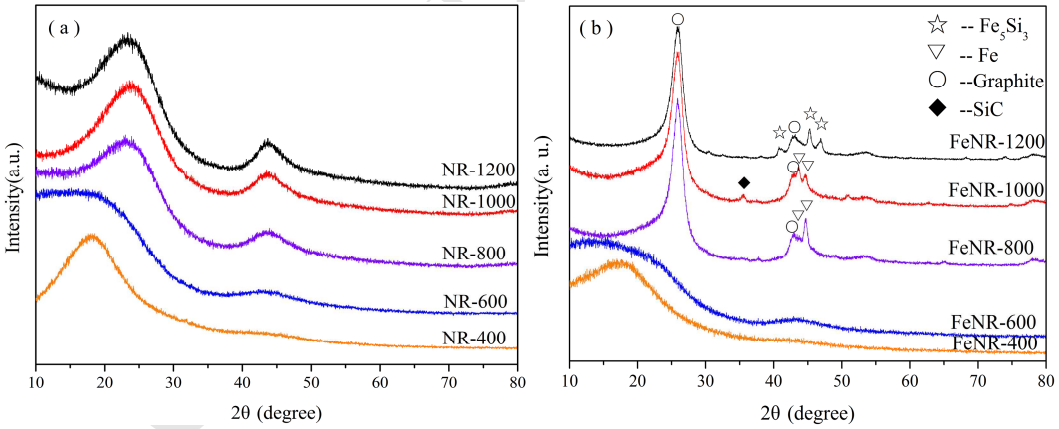

Fig. 7 The XRD spectra of cured NR and cured FeNR-7.5 pyrolyzed at different temperatures: (a) NR; (b) FeNR-7.5.

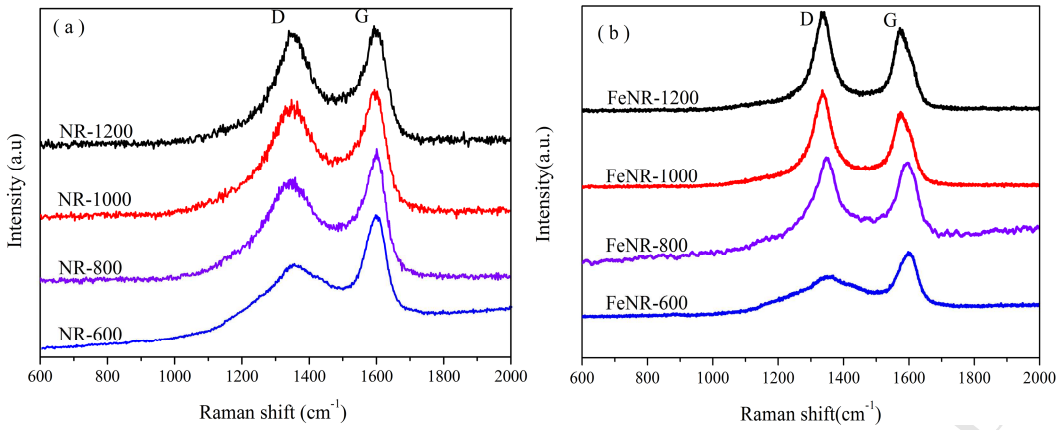

Fig. 8 Raman spectra of (a) cured NR; (b) cured FeNR-7.5 pyrolyzed at 600 °C, 800°C, 1000°C and 1200°C.

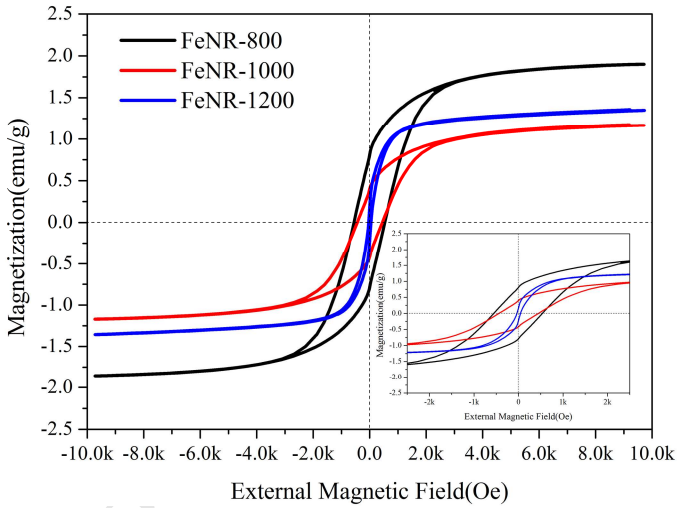

Fig. 9 Magnetic hysteresis loops of sample FeNR-800, FeNR-1000, and FeNR-1200 at 300 K (inset: enlarged portion of the plots at low H)

Table1 TGA data of the cured NR and cured FeNR

Resin	$T_{5\%}$/°C	$T_{10\%}$/°C	T_{max}/°C	C_{800}/°C	C_{1000}/°C	C_{1200}/°C
NR	238.5	410.3	518.8	61.17	48.94	36.35
FeNR-5	298.2	401.6	577.5	66.37	58.41	48.06
FeNR-7.5	303.9	425.1	528.5	69.99	63.17	56.34
FeNR-10	309.3	420.0	548.7	67.59	59.96	50.31
FeNR-12.5	314.9	423.7	527.8	67.25	58.61	51.83

Table 2 Char yields of novolac resin modified with different additives at 800 °C

Additive	C_{800} of neat novolac resin (%)	C_{800} of modified novolac resin(%)	Additive content [a] (wt %)	Increase (%)	References
Clay	60.0	65.0	4.2	5.0	[49]
GO	55.3	63.3	1.0	8.0	[50]
Phenylboronic acid	62.6	67.9	38.9	5.4	[5]
KH560, PTMS, DMDMS	60.0	71.0	69.2	11.0	[51]
Methyltrimetho -xysilane	67.5	72.5	131.7	5.0	[12]
Methyltrimetho -xysilane, BA	67.5	73.0	----- [b]	5.5	[52]

[a] Additive content is the weight ratio of modifier to neat novolac resin.

[b] There are no accurate values shown in reference.

Table 3 XRD and Raman Spectra results of cured NR and FeNR-7.5 treated at different temperatures

Resin	Temperature/^{o}C	2(002)/°	d_{002}-spacing/nm	D-band/cm^{-1}	G-band/cm^{-1}	R
NR	800	23.06	0.3853	1338	1601	2.262
	1000	23.65	0.3759	1339	1595	2.060
	1200	23.38	0.3801	1345	1597	1.846
FeNR-7.5	800	25.88	0.3440	1347	1590	1.650
	1000	25.91	0.3436	1335	1576	1.473
	1200	25.88	0.3440	1337	1578	1.339